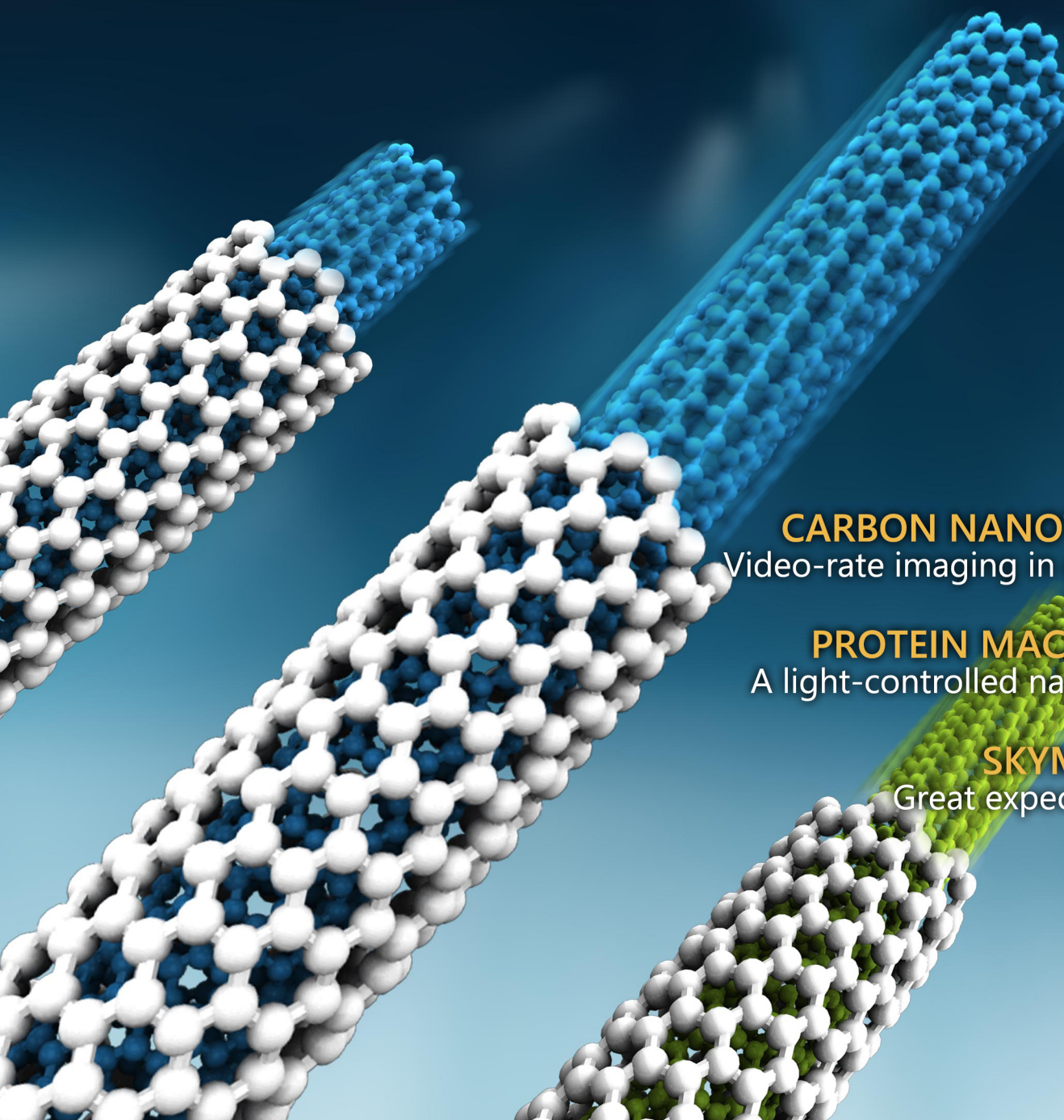


nature

DECEMBER 2013 VOL 8 NO 12
www.nature.com/naturenanotechnology

nanotechnology

Superlubricity goes a long way



CARBON NANOTUBES

Video-rate imaging in devices

PROTEIN MACHINES

A light-controlled nanocage

SKYMIONS

Great expectations

Superlubricity in centimetres-long double-walled carbon nanotubes under ambient conditions

Rufan Zhang¹, Zhiyuan Ning², Yingying Zhang^{3*}, Quanshui Zheng³, Qing Chen², Huanhuan Xie^{1,3}, Qiang Zhang¹, Weizhong Qian¹ and Fei Wei^{1*}

Friction and wear are two main causes of mechanical energy dissipation and component failure, especially in micro/nano-mechanical systems with large surface-to-volume ratios. In the past decade there has been an increasing level of research interest regarding superlubricity^{1–5}, a phenomenon, also called structural superlubricity, in which friction almost vanishes between two incommensurate solid surfaces^{2,3}. However, all experimental structural superlubricity has been obtained on the microscale or nanoscale, and predominantly under high vacuum. Here, we show that superlubricity can be realized in centimetres-long double-walled carbon nanotubes (DWCNTs) under ambient conditions. Centimetres-long inner shells can be pulled out continuously from such nanotubes, with an inter-shell friction lower than 1 nN that is independent of nanotube length. The shear strength of the DWCNTs is only several pascals, four orders of magnitude lower than the lowest reported value in CNTs and graphite. The perfect structure of the ultralong DWCNTs used in our experiments is essential for macroscale superlubricity.

Friction is present in numerous physical phenomena, at all length scales. Sometimes it is exploited to improve our lives, but in many cases it is necessary to decrease it in order to reduce mechanical energy dissipation and surface wear. About one-third to one-half of the world's primary energy is dissipated in mechanical friction^{6,7}, and 80% of machinery component failure is caused by wear⁸. Friction and wear are also problems in micro- and nanomechanical systems with sliding components with high surface-to-volume ratios. The key to solving these issues is superlubricity⁹. Two main types of solid superlubricity can be defined, according to their origin: (1) incommensurate crystalline contact-based superlubricity, which is the original definition of superlubricity and also known as structural superlubricity^{1–5}, and (2) disordered solid interface-based superlubricity^{9–13}. A typical material demonstrating the second type of superlubricity is diamond-like carbon (DLC) film, which can be fabricated with dimensions on the scale of square millimetres, although friction tests have only been conducted for sizes in the range of hundreds of micrometres^{9,13}. In this Letter, 'superlubricity' only refers to 'structural superlubricity' unless otherwise specified. To date, most superlubricity has been realized at the nanoscale under high vacuum^{1–5}. It was believed that macroscale superlubricity did not exist due to the structural deformation of materials at large scale¹. The latest breakthrough in superlubricity was made with a microscale graphite mesa ($10 \times 10 \mu\text{m}^2$)¹⁴. Although superlubricity based on disordered interfaces has been observed in DLC films of macroscale size (several square millimetres), the contact size for the friction test was only several hundred micrometres^{9,13}. Accordingly, superlubricity on the macroscale has yet to be demonstrated.

Multiwalled carbon nanotubes (MWCNTs) composed of coaxial cylindrical graphene layers with a high aspect ratio are ideal candidates for the study of superlubricity. The MWCNT shells can slide or rotate with respect to one another^{15–18}. Because of the difficulty of performing nanomanipulation, in the past two decades there have only been a few experimental reports^{15,19–23} on the sliding or rotational behaviour of MWCNT shells. The measured intershell friction was much higher than theoretical values due to the presence of defects or deformations in the MWCNTs^{17,21,24–26}. The manipulation of individual CNTs is also a challenge because of their nanosize diameters.

The recent breakthrough in producing centimetres-long double-/triple-walled CNTs with perfect atomic structures^{27–29} offers the possibility to explore superlubricity on the macroscale. Figure 1a,b,c and Supplementary Fig. S1 show as-grown, ultralong, double-walled CNTs (DWCNTs) with perfect structures on a silicon substrate (with a 500-nm-thick SiO₂ layer on the surface). To facilitate the manipulation of individual DWCNTs, trenches were fabricated on the silicon substrate. TiO₂ nanoparticles were found to be ideal indicators to 'see' individual CNTs with optical microscopes^{29,30}. Suspended individual DWCNTs decorated with TiO₂ nanoparticles are presented in Fig. 1d,e. These were visible even under an optical microscope (Fig. 1f,i–iii). When a suspended DWCNT was blown by a steady gas flow, it elongated to form a curve. With an increase in gas velocity, the distance between two adjacent TiO₂ nanoparticles on the DWCNT showed a sharp increase, indicating the inner shell of the DWCNT was partly extracted (Fig. 1f,II,ii). Once the gas flow was cut off, the extracted inner shell immediately retracted into the outer shell, indicating ultralow friction between the DWCNT shells (Fig. 1f,III,iii). (For a similar phenomenon see Supplementary Fig. S2.) The pull-out and retraction of the inner shells of MWCNTs have been observed previously in nano- and micrometre-long CNTs under high vacuum^{18,19,31}. However, the CNTs used here were up to 2 cm long and the sliding length of the inner shells for each side was at least 1 cm. This remarkable advance is attributed to the extremely low defect concentration of our CNTs^{19,24,27,29}. This is the first experimental observation of intershell sliding in centimetres-long CNTs under ambient conditions.

The DWCNT inner-shell pull-out experiment was carried out in a scanning electron microscope (SEM) equipped with nanomanipulators. A probe was used to pull out the inner shells (Fig. 2a–e, Supplementary Figs S3, S4). The TiO₂ nanoparticles play a key role in monitoring the abovementioned process. When the probe moved, the suspended DWCNT was elongated to a critical strain, at which point the outer shell broke and remained in a free state (the TiO₂ nanoparticle indicated in Fig. 2f,g did not move). The

¹Beijing Key Laboratory of Green Chemical Reaction Engineering and Technology, Department of Chemical Engineering, Tsinghua University, Beijing 100084, China, ²Key Laboratory for the Physics & Chemistry of Nanodevices, Peking University, Beijing 100871, China, ³Center for Nano and Micro Mechanics, Tsinghua University, Beijing 100084, China. *e-mail: yingyingzhang@tsinghua.edu.cn; wf-dce@tsinghua.edu.cn

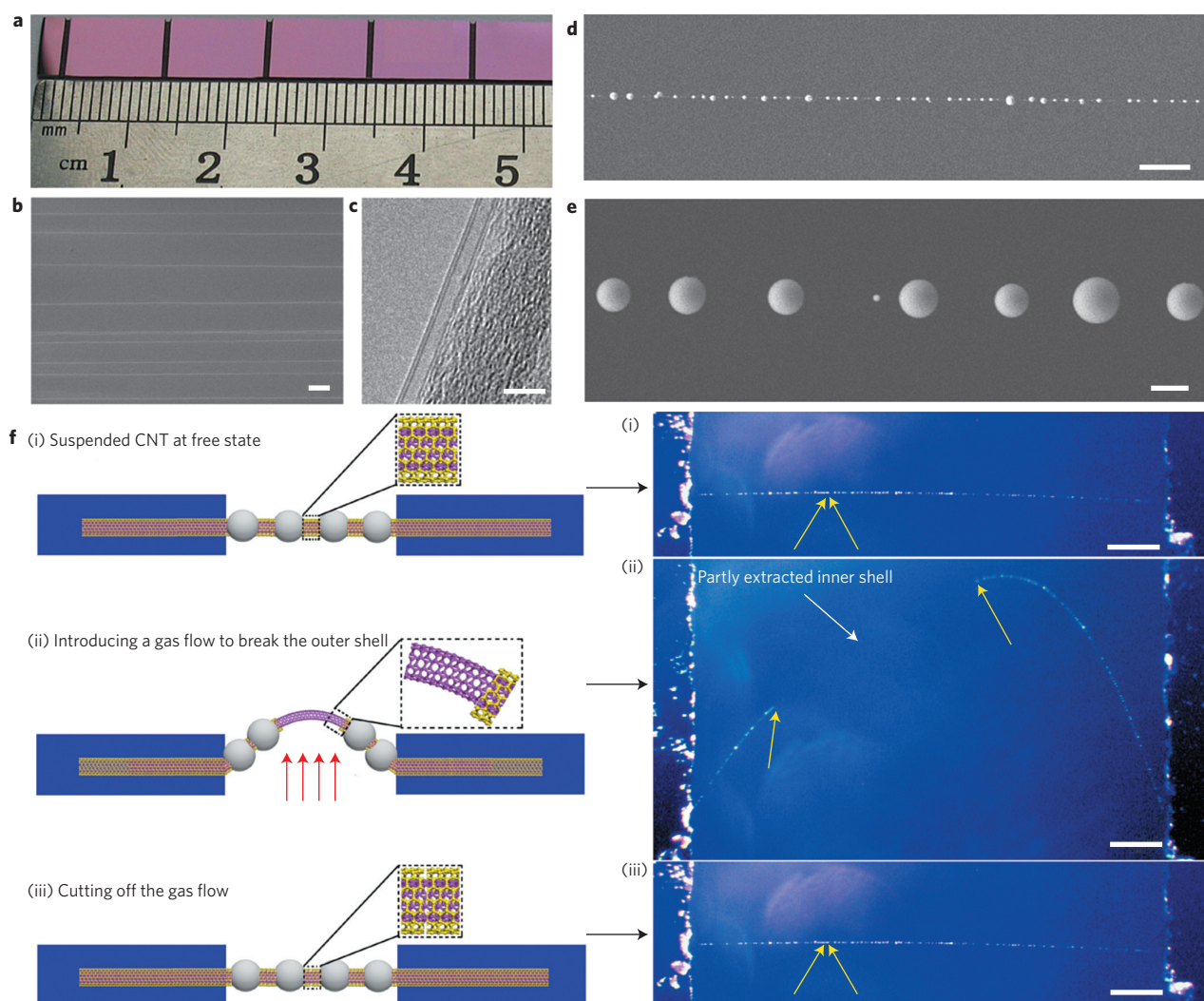


Figure 1 | Observation of inner-shell sliding in ultralong DWCNTs. **a**, Optical image of a Si/SiO₂ substrate with many trenches for growing ultralong CNTs. **b**, SEM image of as-grown ultralong CNTs (scale bar, 200 μm). **c**, TEM image of a DWCNT (scale bar, 5 nm). **d,e**, SEM images of suspended CNTs deposited with TiO₂ nanoparticles (scale bars, 10 μm (**d**) and 1 μm (**e**)). **f**, Illustrations (left) and optical images (right) showing inner-shell sliding processes for ultralong DWCNTs (scale bars in (i)–(iii), 100 μm). Yellow arrows in (i)–(iii) indicate the TiO₂ nanoparticles at the breaking point of the outer shell.

inner shell could be pulled out of the DWCNT continuously. This process could also be conducted under an optical microscope (Supplementary Fig. S5).

To measure the intershell friction of the DWCNTs, a silicon nanorod was used as a force cantilever. The extracted inner shell was first transferred from the probe to the force cantilever (Fig. 2h), and the inner shell was then pulled out by moving the cantilever. The deformation of the cantilever was recorded and the DWCNT intershell friction could be obtained. As shown in Fig. 2i, the deformation of the force cantilever remained identical throughout the above process, indicating that the intershell friction of the DWCNT is independent of the overlap length¹⁶. Figure 2j,k shows that a 10.59-mm-long inner shell was pulled out, which is at least 50 times longer than the previous longest one obtained from a MWCNT²³.

The intershell frictions of three DWCNTs are shown in Fig. 3a. The detailed sliding behaviour of inner shells in DWCNTs is provided in Supplementary Discussion S1 and Supplementary Fig. S6. Even the highest friction is less than 5 nN when pulling a centimetre-long inner shell out of a DWCNT, indicating the macro-scale superlubricity of the DWCNTs. It has been widely accepted that the intershell interaction of CNTs is predominantly composed

of van der Waals forces, which is a π - π^* interaction in nature^{15,16,19,21,31}. Theoretically, the van der Waals forces between CNT shells can be calculated using $F_{\text{vdW}} = -\gamma C = -0.16C$, where γ is the intershell cohesive energy density for a single shell and C is the circumference of the critical shell^{15,32,33}. For a perfect DWCNT without any deformation or defects, the intershell friction is dependent only on its outer diameter¹⁶. The calculated van der Waals forces for the three DWCNTs shown in Fig. 3a are 1.37, 1.47 and 1.64 nN, respectively. The measured friction is ~ 5 –100 times lower than values reported previously^{15,19,21,23}. The dissipation energy during the pull-out process for the three DWCNTs is shown in Fig. 3b. Based on the dissipation energy, we obtained the specific surface energy of these DWCNTs, with values of ~ 0.181 – 0.263 J m^{-2} (average of 0.218 J m^{-2}), which is slightly higher than the theoretical value (~ 0.14 – 0.2 J m^{-2} ; we take 0.18 J m^{-2} as an average)^{19,34}, but much lower than the previously reported experimental values (~ 0.45 – 0.67 J m^{-2})²¹. According to the conventional definition of shear strength, $\tau = F/A = f/\pi DL$, where τ is the shear strength, f is the intershell friction, D is the outer diameter, and L is the overlap length of the DWCNT shells, and if we take the average intershell friction to be 2 nN, the calculated shear strength for pulling a 9-mm-long inner shell out

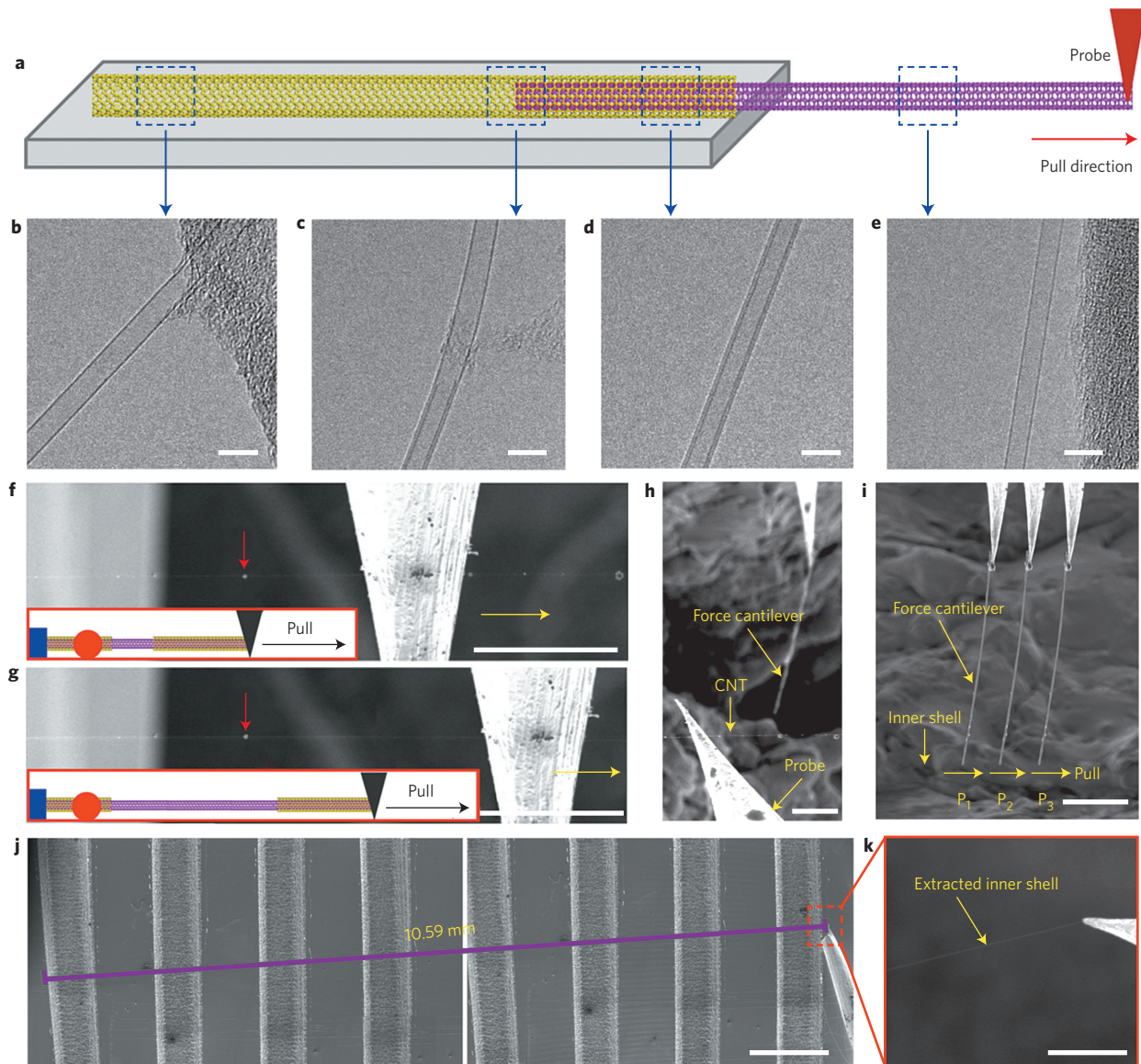


Figure 2 | Process of pulling out the inner shell from a DWCNT. **a**, Schematic of an inner shell being pulled out of a DWCNT. **b–e**, TEM images of different parts of the DWCNT in **a** (scale bars, 5 nm). **f, g**, Process of pulling the inner shell from a DWCNT with a probe (scale bar, 10 μm). The TiO_2 nanoparticle (indicated by red arrows) was on the outer shell and remained unmoved during the pull-out of the inner shell. Insets: illustration of the pull-out process. **h**, Transferring the end of the extracted inner shell from a probe to a force cantilever (scale bar, 5 μm). **i**, Measurement of the intershell friction of the DWCNT using a force cantilever with known K value (scale bar, 10 μm). P_1 , P_2 and P_3 indicate three positions of the force cantilever during the inner-shell pull-out process. **j**, A 10.59-mm-long inner shell was pulled out from the DWCNT (scale bar, 1 mm). **k**, High-resolution SEM image of the extracted inner shell (indicated by the red square in **j**). Scale bar, 5 μm .

of a DWCNT with outer diameter of 2.73 nm (1#) will be as low as 2.6 Pa, at least four orders of magnitude lower than the latest reported value (0.04 MPa) for MWCNTs¹⁹ and graphite¹⁴. The ultralow intershell friction and shear strength realized in centimetre-long DWCNTs proves the existence of superlubricity at macroscale lengths, even under ambient conditions (Fig. 1f). Besides, as shown in Fig. 3a, there are fluctuations in the measured intershell friction, the origins of which are discussed in Supplementary Discussion S2.

The origins of superlubricity in DWCNTs can be explained in two ways. On the one hand, the interface between the shells of DWCNTs should be incommensurate. In other words, the two surfaces have no energetically preferred position with respect to one another, and so can slide relative to each other with no cost in energy⁹. It is known that the CNT shells can be viewed as rolled-up graphite sheets, and their structures can be expressed by a

chiral index (n, m). For DWCNTs, the (n, m) indices of different shells are independent of one another. Only if the inner and outer shells meet the lattice matching requirement (armchair@armchair or zigzag@zigzag) can they satisfy the AB stacking for commensurate contact between two graphene sheets^{9,14,27,35,36} (for a detailed discussion of the effect of the chirality of the DWCNTs on their intershell friction, see Supplementary Discussion S3). Accordingly, the shells of most as-grown DWCNTs are in incommensurate contact. On the other hand, the superlubricity of DWCNTs can be understood in terms of the length-independent van der Waals interaction between the shells. As shown in Fig. 4a, for an ideal DWCNT with a partly extruded inner shell, the van der Waals interaction between the inner and outer shells can be divided into two sections. In the overlapped section (section I in Fig. 4a), the shear stress vanishes due to the repetitive breaking and reforming of van der Waals interaction between adjacent shells¹⁶. Thus, only

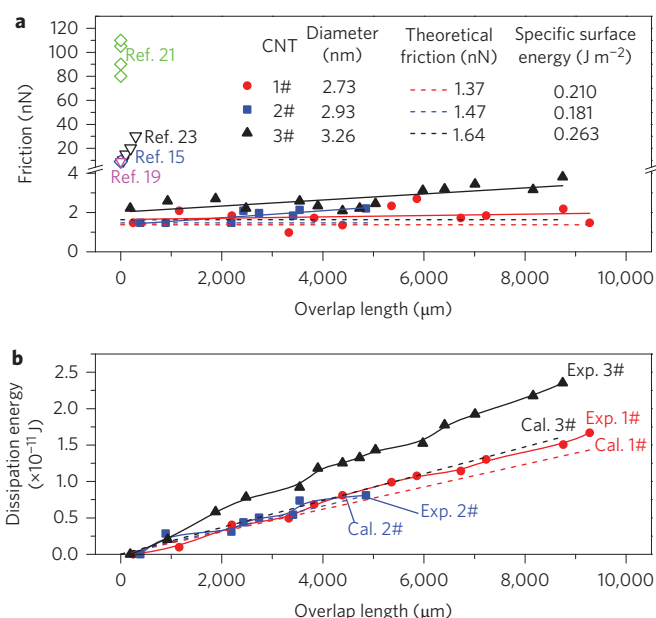


Figure 3 | Friction and dissipation energy of three DWCNTs. **a**, Intershell friction of three DWCNTs with different outer diameters, as well as published data^{15,19,21,23} for comparison. Inset: specific surface energies of the three DWCNTs. **b**, Dissipative energy of the three DWCNTs during the inner-shell pull-out process (cal., calculated dissipation energy, where the special surface energy was taken to be 0.18 J m⁻² (ref. 17); exp., experimental value).

the edge section (section II) is responsible for the intershell interaction in DWCNTs during the pulling-out process. Theoretically, the variation of the total van der Waals interaction only depends on the crucial edge of the outer shell and ultimately depends on the outer diameter of the DWCNT. In addition, the perfect structure (Fig. 1f, Supplementary Fig. S1) of the as-grown CNTs plays a key role in the existence of macroscale superlubricity in centimetres-long DWCNTs. The presence of defects would significantly increase the intershell interaction of MWCNTs (for a detailed discussion see Supplementary Discussion S4). The ultralow friction observed here is rooted in the perfect structure of our ultralong CNTs^{27–29}, as well as in the relative straightness of the DWCNTs (Fig. 1b). As shown in Fig. 4b,c, the axial curvature significantly affects the intershell interaction in DWCNTs. For the five DWCNTs with different axial curvatures shown in Fig. 4b, it is obvious that the intershell friction of a DWCNT with large curvature is higher than that of DWCNTs with small curvature (Fig. 4c) (for detailed discussions see Supplementary Discussion S5 and Supplementary Figs S7, S8).

In summary, we have observed superlubricity in centimetres-long DWCNTs with perfect structures under ambient conditions. Intershell friction was measured during the process of pulling out inner shells from centimetres-long DWCNTs. The intershell friction was independent of pull-out length and could be as low as 1 nN. The shear strength of the DWCNTs was only several pascals, four orders of magnitude smaller than the best reported value reported to date¹⁴. The superlubricity in our DWCNTs can be understood in terms of the absence of defects and large axial curvatures in the used DWCNTs as well as the length-independent variation of the van der Waals interaction between the CNT shells during the pull-out process.

Methods

CNT synthesis. A solution containing catalyst precursor FeCl₃ in ethanol (0.03 mol l⁻¹) was deposited onto a silicon substrate using a microprinting method. After reduction in H₂ and argon (H₂:Ar = 2:1 by volume, with a total flow of 200 s.c.c.m.) at 900 °C for 25 min, the iron precursor became iron nanoparticles,

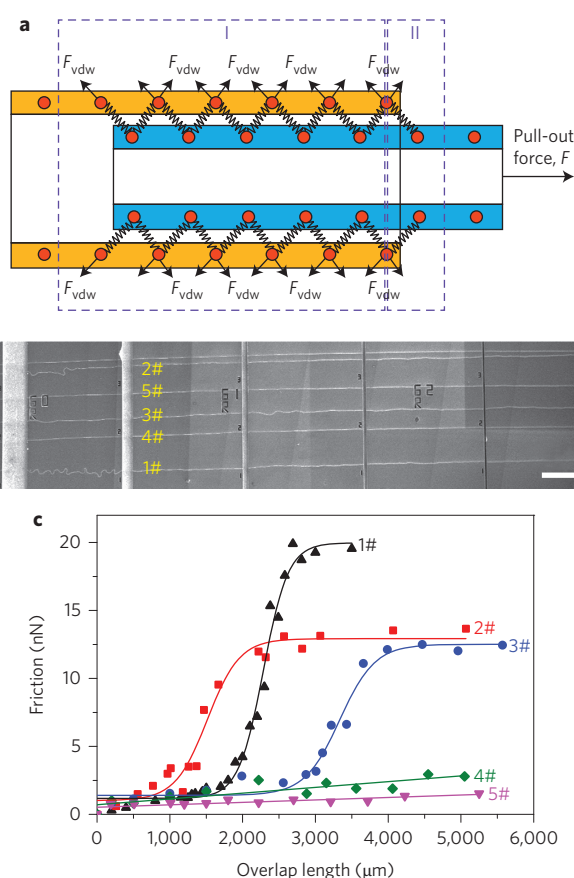


Figure 4 | Analysis of intershell friction of DWCNTs. **a**, Interaction between the inner and outer shells of a DWCNT during the inner-shell pull-out process. The forces are composed of van der Waals interactions between the two shells. Scale bar, 200 μm. **b**, SEM image of ultralong MWCNTs with different axial curvatures. **c**, Measured friction for the five ultralong MWCNTs shown in **b**.

which worked as catalysts for the subsequent chemical vapour deposition of CNTs at 1,000 °C. CH₄ mixed with H₂ (CH₄:H₂ = 1:2 by volume, with a total flow of 75 s.c.c.m.) was used as the carbon source, together with 0.43% H₂O for accelerating CNT growth. The growth time for the CNTs was usually 10–20 min, depending on the length of CNT desired.

Deposition of TiO₂ nanoparticles on CNTs. The deposition process was conducted in a fume hood, with a humidity controller to regulate and measure the relative air humidity. The substrates with suspended CNTs were placed in contact with TiCl₄ vapour and TiO₂ smog under ambient conditions to deposit TiO₂ nanoparticles. The contact time usually ranged from 3.0 s to 7.0 s. Substrates with suspended CNTs were removed to halt the deposition process.

Characterization. The CNTs were characterized by SEM (JSM 7401F, 1.0 kV; FEI, XL30F, 3 kV), high-resolution transmission electron microscopy (TEM; JEM-2010, 120.0 kV) and a Raman instrument (Horiba HR 800, 632.8 nm). An optical microscope (long-working-distance metallography microscope, FS-70Z) was used for optical characterization and manipulation of individual CNTs.

Experimental set-up for manipulating individual CNTs. The manipulation of individual CNTs was conducted using a four-nanoprobe system (MM3A nanoprobe, Kleindiek Company) inside an FEI XL30F SEM (Supplementary Fig. S3a–c). The movement of a nanoprobe arm, with a tungsten probe mounted on it, was driven by two perpendicular rotation motors (RM-1 and RM-2, Supplementary Fig. S3d). One motor controlled the horizontal rotation of the arm, and the other controlled the vertical rotation using spherical coordinates. The two motors enabled the arm to move on a surface of a sphere with an accuracy of ~2.5 nm. The radial movement of the tungsten probe, which was mounted at the end of the arm, was controlled by an additional motor, which drove the radial motion of the arm (the finest step of this radial motion was 0.25 nm). The range of the rotation motor could be above 180°, while that of the radial motion was 12 mm. All three motors could be driven with varying speed, and no noticeable creeping or delayed motion was observed when decreasing the speed. To measure the nanoscale forces of the intershell friction of the

CNTs, a silicon nanorod was mounted onto the tungsten probe as a force cantilever (Supplementary Fig. S3f). This system could be used to manipulate the CNTs in a convenient and controlled way.

Intershell friction measurement. A silicon nanorod (35 μm in length, 200 nm in diameter) was used as the force cantilever (force constant $K \approx 1\text{--}10 \text{ nN } \mu\text{m}^{-1}$, as precisely measured using an electric field-induced resonance method³⁷). The force cantilever was fixed onto the tungsten probe attached on the nanoprobe arm (Supplementary Fig. S3f). Once the outer shell of the MWCNT was broken and the inner shell pulled out, the extracted inner shell was transferred from the probe to the force cantilever, and the inner shell was fixed onto the force cantilever by depositing some amorphous carbon onto their point of contact. The inner shell could then be continuously pulled out by moving the force cantilever. The deformation of the force cantilever was recorded and the corresponding pulling force could be obtained by multiplying the deformation by K .

Received 12 March 2013; accepted 19 September 2013;
published online 3 November 2013

References

- Dienwiebel, M. *et al.* Superlubricity of graphite. *Phys. Rev. Lett.* **92**, 126101 (2004).
- Hirano, M. & Shinjo, K. Atomistic locking and friction. *Phys. Rev. B* **41**, 11837 (1990).
- Hirano, M., Shinjo, K., Kaneko, R. & Murata, Y. Anisotropy of frictional forces in muscovite mica. *Phys. Rev. Lett.* **67**, 2642–2645 (1991).
- Hirano, M., Shinjo, K., Kaneko, R. & Murata, Y. Observation of superlubricity by scanning tunneling microscopy. *Phys. Rev. Lett.* **78**, 1448–1451 (1997).
- Martin, J., Donnet, C., Le Mogne, T. & Epicier, T. Superlubricity of molybdenum disulphide. *Phys. Rev. B* **48**, 10583 (1993).
- Szeri, A. Z. *Tribology: Friction, Lubrication, and Wear* (Hemisphere, 1980).
- Amiri, M. & Khonsari, M. M. On the thermodynamics of friction and wear—a review. *Entropy* **12**, 1021–1049 (2010).
- Yunhui, M., Dehua, T., Xicheng, W. & Qinghua, L. Research on friction-coatings with activated ultra-thick tin-base. *Adv. Tribol.* 915–919 (2010).
- Erdemir, A. & Martin, J. M. *Superlubricity* (Elsevier, 2007).
- Andersson, J., Erck, R. & Erdemir, A. Friction of diamond-like carbon films in different atmospheres. *Wear* **254**, 1070–1075 (2003).
- Erdemir, A. & Donnet, C. Tribology of diamond-like carbon films: recent progress and future prospects. *J. Phys. D* **39**, R311 (2006).
- Sokoloff, J. Theory of the effects of multiscale surface roughness and stiffness on static friction. *Phys. Rev. E* **73**, 016104 (2006).
- Erdemir, A., Eryilmaz, O. & Fenske, G. Synthesis of diamondlike carbon films with superlow friction and wear properties. *J. Vac. Sci. Technol. A* **18**, 1987–1992 (2000).
- Liu, Z. *et al.* Observation of microscale superlubricity in graphite. *Phys. Rev. Lett.* **108**, 205503 (2012).
- Cummings, J. & Zettl, A. Low-friction nanoscale linear bearing realized from multiwall carbon nanotubes. *Science* **289**, 602–604 (2000).
- Li, Y. *et al.* Molecular mechanics simulation of the sliding behavior between nested walls in a multi-walled carbon nanotube. *Carbon* **48**, 2934–2940 (2010).
- Xia, Z. & Curtin, W. Pullout forces and friction in multiwall carbon nanotubes. *Phys. Rev. B* **69**, 233408 (2004).
- Zheng, Q. & Jiang, Q. Multiwalled carbon nanotubes as gigahertz oscillators. *Phys. Rev. Lett.* **88**, 45503 (2002).
- Kis, A., Jensen, K., Aloni, S., Mickelson, W. & Zettl, A. Interlayer forces and ultralow sliding friction in multiwalled carbon nanotubes. *Phys. Rev. Lett.* **97**, 25501 (2006).
- Fennimore, A. *et al.* Rotational actuators based on carbon nanotubes. *Nature* **424**, 408–410 (2003).
- Yu, M. F., Yakobson, B. I. & Ruoff, R. S. Controlled sliding and pullout of nested shells in individual multiwalled carbon nanotubes. *J. Phys. Chem. B* **104**, 8764–8767 (2000).
- Yu, M. F. *et al.* Strength and breaking mechanism of multiwalled carbon nanotubes under tensile load. *Science* **287**, 637–640 (2000).
- Hong, B. H. *et al.* Extracting subnanometer single shells from ultralong multiwalled carbon nanotubes. *Proc. Natl Acad. Sci. USA* **102**, 14155–14158 (2005).
- Guo, W., Zhong, W., Dai, Y. & Li, S. Coupled defect-size effects on interlayer friction in multiwalled carbon nanotubes. *Phys. Rev. B* **72**, 075409 (2005).
- Huhtala, M. *et al.* Improved mechanical load transfer between shells of multiwalled carbon nanotubes. *Phys. Rev. B* **70**, 045404 (2004).
- Peng, B. *et al.* Measurements of near-ultimate strength for multiwalled carbon nanotubes and irradiation-induced crosslinking improvements. *Nature Nanotech.* **3**, 626–631 (2008).
- Wen, Q. *et al.* 100 nm long, semiconducting triple-walled carbon nanotubes. *Adv. Mater.* **22**, 1867–1871 (2010).
- Wen, Q. *et al.* Growing 20 cm long DWNTs/TWNTs at a rapid growth rate of 80–90 $\mu\text{m/s}$. *Chem. Mater.* **22**, 1294–1296 (2010).
- Zhang, R. *et al.* Superstrong ultralong carbon nanotubes for mechanical energy storage. *Adv. Mater.* **23**, 3387–3391 (2011).
- Zhang, R. *et al.* Optical visualization of individual ultralong carbon nanotubes by chemical vapour deposition of titanium dioxide nanoparticles. *Nature Commun.* **4**, 1727 (2013).
- Zheng, Q., Liu, J. Z. & Jiang, Q. Excess van der Waals interaction energy of a multiwalled carbon nanotube with an extruded core and the induced core oscillation. *Phys. Rev. B* **65**, 245409 (2002).
- Kis, A. & Zettl, A. Nanomechanics of carbon nanotubes. *Phil. Trans. R. Soc. Lond. A* **366**, 1591–1611 (2008).
- Benedict, L. X. *et al.* Microscopic determination of the interlayer binding energy in graphite. *Chem. Phys. Lett.* **286**, 490–496 (1998).
- Gnecco, E., Bennewitz, R., Gyalog, T. & Meyer, E. Friction experiments on the nanometre scale. *J. Phys.* **13**, R619–R641 (2001).
- Ding, F., Harutyunyan, A. R. & Yakobson, B. I. Dislocation theory of chirality-controlled nanotube growth. *Proc. Natl Acad. Sci. USA* **106**, 2506–2509 (2009).
- Xu, Z., Li, X., Yakobson, B. I. & Ding, F. Interaction between graphene layers and the mechanisms of graphite's superlubricity and self-retraction. *Nanoscale* **5**, 6736–6741 (2013).
- Wei, X. L., Liu, Y., Chen, Q., Wang, M. S. & Peng, L. M. The very-low shear modulus of multi-walled carbon nanotubes determined simultaneously with the axial Young's modulus via *in situ* experiments. *Adv. Funct. Mater.* **18**, 1555–1562 (2008).

Acknowledgements

This work was supported by the Foundation for the National Basic Research Program of China (Program Number 2011CB932602 and 2013CB934200) and the National Natural Science Foundation of China (Grant Number 51372132 and 60925003). The authors thank Dezheng Wang and Wengen Ou-Yang for helpful discussions.

Author contributions

F.W. proposed and supervised the project. R.F.Z. designed and performed the experiments and wrote the manuscript. Y.Y.Z. co-supervised the project and designed the outline of the manuscript. Z.Y.N. participated in most experiments. Q.S.Z., Q.S., Q.Z. and Q.W.Z. participated in data analysis and manuscript preparation. H.H.X. participated in the synthesis of ultralong CNTs.

Additional information

Supplementary information is available in the online version of the paper. Reprints and permissions information is available online at www.nature.com/reprints. Correspondence and requests for materials should be addressed to Y.Z. and F.W.

Competing financial interests

The authors declare no competing financial interests.